Materials Characterization 136 (2018) 302–309

Contents lists available at ScienceDirect

Materials Characterization

journal homepage: www.elsevier.com/locate/matchar

A new tetragonal phase in CoFeCrGe Heusler alloy

Y.-L. Jin[a,b], X.-Z. Li[a,*], D.J. Sellmyer[a,b]

[a] Nebraska Center for Materials and Nanoscience, University of Nebraska, Lincoln, NE 68588, USA
[b] Department of Physics and Astronomy, University of Nebraska, Lincoln, NE 68588, USA

ARTICLE INFO

Keywords:
CoFeCrGe
Heusler alloy
Crystal structure
TEM
SAED
HREM

ABSTRACT

CoFeCrGe ribbons were prepared by melt spinning and then annealed at 300 °C for 4 h and 500 °C for 4 h, respectively. The as-spun ribbons of CoFeCrGe have the B2 type structure with $a = 0.287$ nm. The CoFeCrGe ribbons annealed at 300 °C are composed mainly of the $L2_1$ type structure with $a = 0.578$ nm in partial disorder and the B2 type structure with $a = 0.289$ nm in further disorder case. The ribbons annealed at 500 °C are composed of three compounds with average compositions of $Co_{26.0}Fe_{26.5}Cr_{23.5}Ge_{24.0}$, $Co_{3.8}Fe_{6.4}Cr_{68.5}Ge_{21.3}$ and $Co_{53.4}Fe_{30.4}Cr_{8.6}Ge_{7.6}$, listed in a sequence of volume percentage from major to minor. The primary compound $Co_{26.0}Fe_{26.5}Cr_{23.5}Ge_{24.0}$ is the $L2_1$-type structure with $a = 0.571$ nm in partial disorder and the B2 type structure with $a = 0.286$ nm in further disorder case. The secondary compound $Co_{3.8}Fe_{6.4}Cr_{68.5}Ge_{21.3}$ has a cubic Cr_3Ge structure with $a = 0.461$ nm. The tertiary compound $Co_{53.4}Fe_{30.4}Cr_{8.6}Ge_{7.6}$ is a new tetragonal structure with lattice parameters $a = 0.76$ nm, $c = 0.284$ nm, which were determined by using tilt-series electron diffraction technique in this work. The tertiary (Co, Fe)-rich phase is usually embedded in the matrix of the secondary Cr-rich phase, but there is no special orientation between the two phases. The difference in the magnetic hysteresis loops of the samples annealed at 300 °C and 500 °C has been interpreted as the appearance of the new tetragonal crystalline phase. Element doping is the possible way for further developing the single tetragonal phase or increasing the amount of this phase.

1. Introduction

Magnetic materials in the class of Heusler compounds such as Co_2CrGe, CoFeCrGe are attracting much attention recently for their potential in spintronic devices. Since the electronic band structure of half-metals is metallic for one spin channel and semiconducting or insulating for the opposite spin channel, they are capable of producing spin currents of only one orientation (100% spin-polarized current) [1–7]. Regular Heusler compounds have the X_2YZ elemental composition, where X and Y are the transition-metal elements and Z is the main-group element and crystallize in the cubic $L2_1$ (prototype Cu_2MnAl) structure. This type of compound may deteriorate into the B2 structure when chemical disorder occurs. Further, some of the Heusler compounds crystallize in tetragonal structure with large perpendicular magnetic anisotropy, showing potential for spin-transport torque (STT)-based memory and permanent-magnet applications as well [8,9]. Quaternary Heusler compounds with elemental composition XX'YZ (prototype LiMgPdSn) also exist basically as the derivatives of X_2YZ compounds with one of the X atoms being replaced by another transition-metal element [10].

Experimental and theoretical investigations of two quaternary alloys CoFeCrSi and CoFeCrGe were reported in prior work [7]. In the CoFeCrGe system, the cubic $L2_1$ structure with partial disorder was found in ribbons annealed at low temperature and a phase decomposition was observed when the samples were annealed above 402 °C. The as-spun and 300 °C-annealed CoFeCrGe samples show ferrimagnetic spin order at room temperature and have Curie temperatures (T_C) significantly above room temperature. The measured saturation magnetization, 535 emu/cm^3 (2.8 μ_B/f. u.), is close to the theoretically predicted value of 3.0 μ_B/f. u. for the half-metallic phase. The saturation magnetization is 672 emu/cm^3 for CoFeCrGe ribbons annealed at 500 °C. Powder X-ray diffraction (XRD) analysis confirmed a phase

* Corresponding author at: Nebraska Center for Materials and Nanoscience, N201 NANO, University of Nebraska, Lincoln, NE 68588, USA.
E-mail address: xzli@unl.edu (X.-Z. Li).

https://doi.org/10.1016/j.matchar.2017.12.036
Received 27 October 2017; Received in revised form 21 December 2017; Accepted 22 December 2017
Available online 23 December 2017
1044-5803/

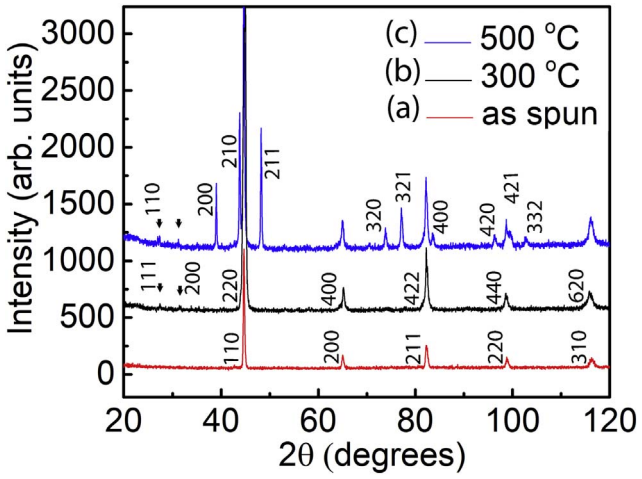

Fig. 1. The XRD diagrams of (a) the as-spun, (b) the 300 °C-annealed and (c) the 500 °C-annealed FeCoCrGe ribbons. The detailed analysis is given in the context. For clarity, the diagrams in (b) and (c) are shifted up, only the indexes of the $L2_1$ structure are labeled in (b) and only the indexes of the Cr-rich (Cr, Fe, Co)$_3$Ge phase are labeled in (c).

decomposition in the 500 °C-annealed CoFeCrGe samples. The diffraction peaks were indexed with two compounds with structural prototypes of Co_2FeGe and Cr_3Ge. However, the rather weak peaks in the XRD diagram of the 500 °C-annealed ribbons cannot be indexed by the $L2_1$ phase or the secondary Cr-rich phases. These suggest the existence of another intermetallic phase in the 500 °C-annealed ribbons.

In the present work, the compositions and structures of the crystalline phases in the annealed samples were systematically characterized by transmission electron microscopy (TEM), energy-dispersive X-ray spectroscopy (EDS), selected-area electron diffraction (SAED) and high-resolution electron image (HREM) experiments. The magnetic measurements of the samples annealed at 300 °C and 500 °C in the previous work [7] are reinterpreted with the results of the crystalline phase analysis.

2. Experimental Methods

Ingots of the equiatomic CoFeCrGe alloy were arc melted from high-purity (99.95%) elements in an argon atmosphere. The ribbons about 2 mm-wide and 50 μm-thick were made by ejecting molten alloys in a quartz tube onto the surface of a copper wheel with tangential wheel speeds of 25 m/s. Two sets of CoFeCrGe ribbons were annealed under high purity of protective argon at 300 °C for 4 h and 500 °C for 4 h, respectively. The magnetic properties were measured using a SQUID magnetometer with applied magnetic field in the ribbon plane.

TEM specimens were prepared by grinding the ribbons into fine powders in ethanol solution and then put a drop of the liquid mixture onto a Cu grid with C film. TEM experiments were performed with a 200 kV Thermo Fisher Scientific (previous FEI) Tecnai Osiris (scanning) transmission electron microscope equipped with the ChemiSTEM system and Bruker's ESPRIT software. The experimental SAED patterns were analyzed using LANDYNE software [11], e.g., SAED3d [12], QSAED [12] and SPICA [13]. SAED3d was used for simulation and analysis of electron-diffraction patterns, QSAED was used for retreating diffraction intensity and SPICA for generating stereographic projection, applicable to specimen orientation adjustment in TEM experiments.

3. Structural Characterization

Structural properties of as-spun CoFeCrGe ribbons and those annealed at two different temperature are shown in Fig. 1. The powder XRD pattern of the as-spun CoFeCrGe ribbons can be indexed with a compound of B2 structure with $a = 0.287$ nm; the powder XRD pattern of the 300 °C-annealed CoFeCrGe ribbons can be indexed with two phases: the $L2_1$ structure with $a = 0.578$ nm in partial chemical disorder and the B2 structure with $a = 0.289$ nm in further disorder case; the powder XRD pattern of the 500 °C-annealed CoFeCrGe ribbons can be indexed with the multiple phases: the primary compound is the $L2_1$ structure with $a = 0.571$ nm in partial chemical disorder and the B2 structure with $a = 0.286$ nm in further disorder case, and the secondary phase is the Cr-rich (Cr, Fe, Co)$_3$Ge phase with $a = 0.461$ nm. However, the rather weak peaks in the XRD diagram of the 500 °C-annealed ribbons cannot be indexed by the $L2_1$ phase or the secondary Cr-rich phases.

3.1. TEM Study of the Main Compound in CoFeCrGe Alloys

Fig. 2 shows the TEM images of the primary compound in the as-spun, 300 °C-annealed and 500 °C-annealed samples, respectively. The grain size increases from about 10 nm in the as-spun samples to several hundred nm in the 300 °C-annealed samples and decreases to about

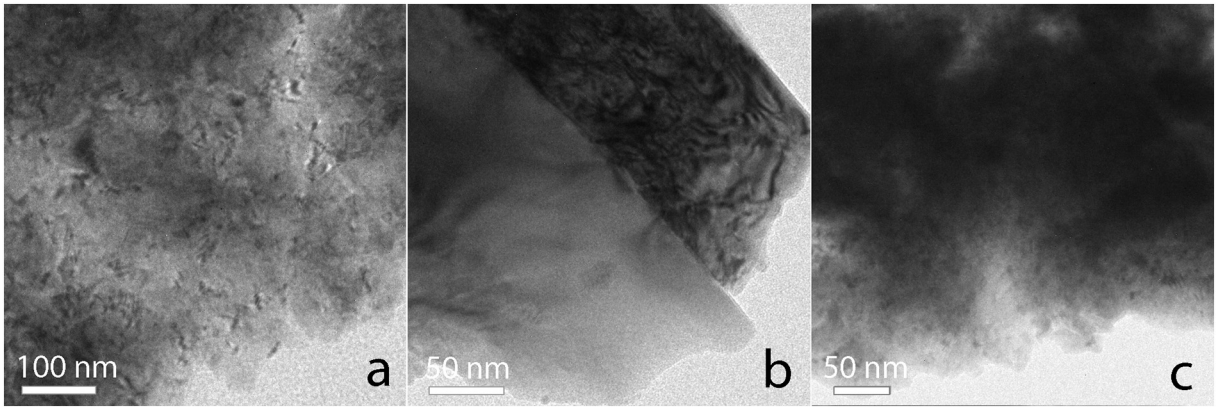

Fig. 2. TEM images of (a) the as-spun, (b) the 300 °C-anneal and (c) the 500 °C-anneal FeCoCrGe ribbons.

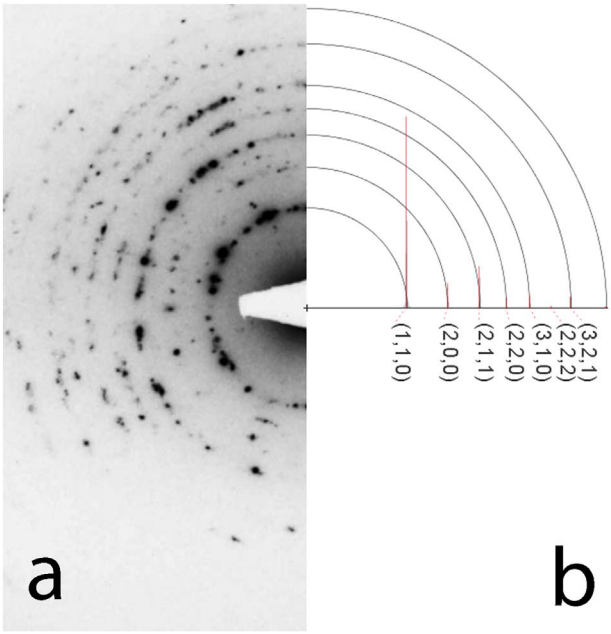

Fig. 3. SAED pattern of the main phase in the as-spun CoFeCrGe ribbons.

5 nm in the 500 °C-annealed samples. The experimental SAED patterns and simulation based the B2 structure are given in Figs. 3–5 for phase identification. The different grain sizes in the as-spun and 500 °C-annealed samples also are reflected in the rings, which show clearly isolated diffraction spots in Fig. 3 and the continuous rings in Fig. 5. EDS analysis confirmed the equiatomic CoFeCrSi composition for all grains in the as-spun and the 300 °C-annealed samples. However, three types of grains have been observed in the 500 °C-annealed samples. The main component is very fine grains whose stoichiometry composition was confirmed to be $Co_{26}Fe_{26.5}Cr_{23.5}Ge_{24}$ near to the equiatomic Heusler alloy. The volume is estimated to be about 48% by counting statistically the grains in multiple TEM samples. The results for the other two components are given in the following sections.

3.2. TEM Study of the Cr-Rich Phase in the 500 °C-Annealed CoFeCrGe Samples

The second type of compound with grain size about several hundred nm up to 1–2 μm and a stoichiometry composition near $Co_{3.8}Fe_{6.4}Cr_{68.5}Ge_{21.3}$ was observed in the 500 °C-annealed samples. The volume is estimated to be about 34% by counting statistically the grains in multiple TEM samples. Fig. 6 shows the TEM image of the Cr-rich cubic phase; the central grain displays darker contrast because the grain was aligned along or near one of the main zone-axes. Fig. 7 shows the SAED patterns of the Cr-rich cubic phase along (a) [100], (b) [111] and (c) [121] zone axes. The SAED patterns were indexed using the cubic Cr_3Ge prototype structure. The results of the SAED analysis are in good agreement with the results of the previous XRD analysis.

3.3. A New Tetragonal Phase in the 500 °C-Annealed CoFeCrGe Samples

Although two compounds in the 500 °C-annealed CoFeCrGe samples were revealed in the previous XRD analysis, the third type of compound with grain size about 200–300 nm and an average composition of $Co_{53.4}Fe_{30.4}Cr_{8.6}Ge_{7.6}$ in over 10 sample grains was observed together with the Cr-rich cubic phase in the 500 °C-annealed samples. The volume is estimated to be about 18% by counting statistically the grains in multiple TEM samples. The compound has been identified as a new tetragonal phase in the present SAED study. Fig. 8 shows the TEM image of the new tetragonal phase in an irregular shape embedded in the grain of the Cr-rich cubic phase. The grain appears in darker contrast because the grain was aligned along or near one of the main zone-axes.

Fig. 9 shows the SAED patterns obtained from multiple experiments and rearranged together from the [001] to the [010] zone axes with the help of the SPICA [13] software. It is notable that the patterns along the [100] and [010] axes are identical, so only the tilt SAED patterns along the [100] zone axis are presented. The experimental tilt angles away from the [001] zone axis are listed with each SAED pattern. The lattice type and parameters were determined by means of the reciprocal lattice reconstruction from a series of tilt SAED patterns, as shown in Fig. 10(a), which is a snapshot of the Launce [12] software. The SAED patterns in Fig. 9(a–e) share common reflections in a row, the

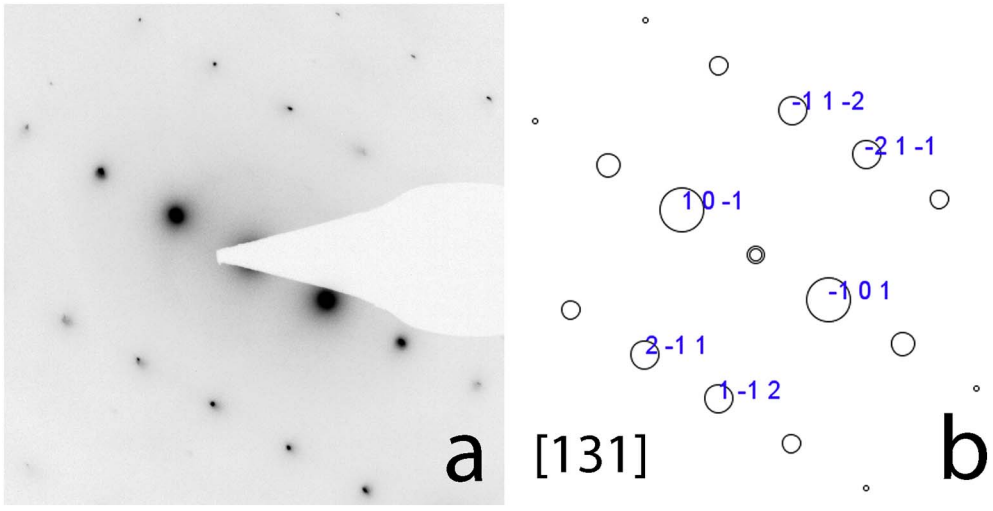

Fig. 4. SAED pattern of the main phase in the 300 °C-annealed CoFeCrGe ribbons.

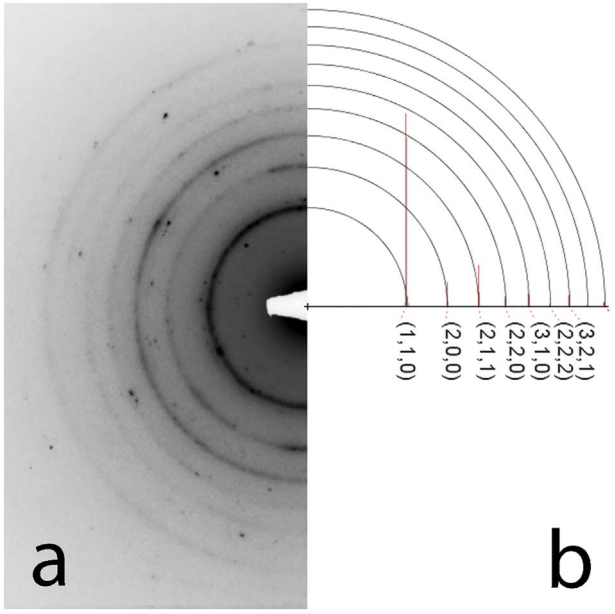

Fig. 5. SAED pattern of the main phase in the 500 °C-annealed CoFeCrGe ribbons.

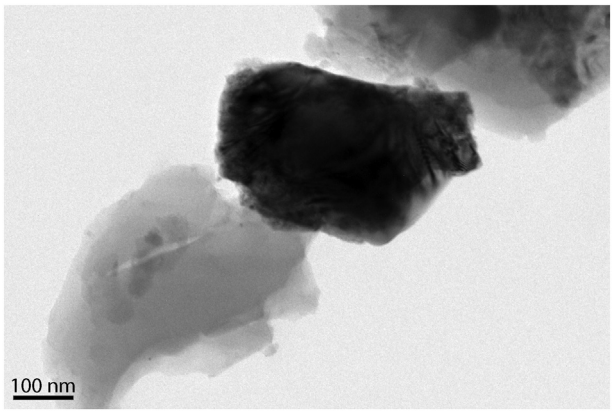

Fig. 6. TEM image of the Cr-rich phase in the 500 °C-annealed CoGeCrGe ribbons.

reflections perpendicular the common row in each SAED pattern were used to build the reciprocal lattice. A tetragonal lattice has been determined with $a = 0.76$ nm, $c = 0.284$ nm. The calculated tilt angles are listed near the experimental data and the zone axes for each SAED pattern are labeled in Fig. 9. Fig. 10(b)shows the distribution of the corresponding zone axes in a stereogram.

It is clear that an extinction occurs among the reflections of (h00) and (0k0) when h, k are odd. The extinct reflections may appear, e.g. in the [001] SAED pattern, due to strong dynamic multiple scattering. Fig. 11 shows (a) the SAED pattern of the [001] zone axis in the relatively thin area and (b) the processed pattern of (a) with the averaged intensity of (h k l) and ($-h$ $-k$ $-l$). The space group is $P42_12$ (90) according to the lattice type and the extinction rule. Fig. 12 shows an HREM image of the new tetragonal phase along the [001] zone axis. A unit cell was marked as the square in the HREM image. The features of the image can be described as circles at each of the square corners. However, the sample was rather thick that the circles only appear along the edge of the grain.

3.4. Relation between the New Tetragonal Phase and the Cr-Rich Cubic Phase

It has been observed that the new tetragonal phase exists in the matrix of the Cr-rich cubic phase. The grains of the tetragonal phase were observed mostly in irregular shapes as shown in Fig. 8, but a grain in a nearly rectangular shape was also observed. Fig. 13 shows (a) the TEM image of the new tetragonal phase and (b) a schematic drawing for the interpretation of the facets of the grain. The darker contrast of the grain is due to the grain being aligned along or near one of the main zone-axes.

The lattice parameters of the two phases do not allow a prefect lattice matching in any form, which indicates that there may be no fixed orientation relationship between them. SAED experiment confirms this suggestion. Fig. 14 shows (a) a SAED pattern along the [110] axis from the new tetragonal phase and (b) a SAED pattern along the [001] zone axis from the adjacent matrix of the Cr-rich cubic phase. There is a tilt angle of 6.8° between the two SAED patterns along their nearest main zone axis.

4. Discussion

4.1. Comparison of the New Tetragonal Phase with Other Crystalline Phases

In order to understand the new tetragonal phase, the Co-rich and Fe-

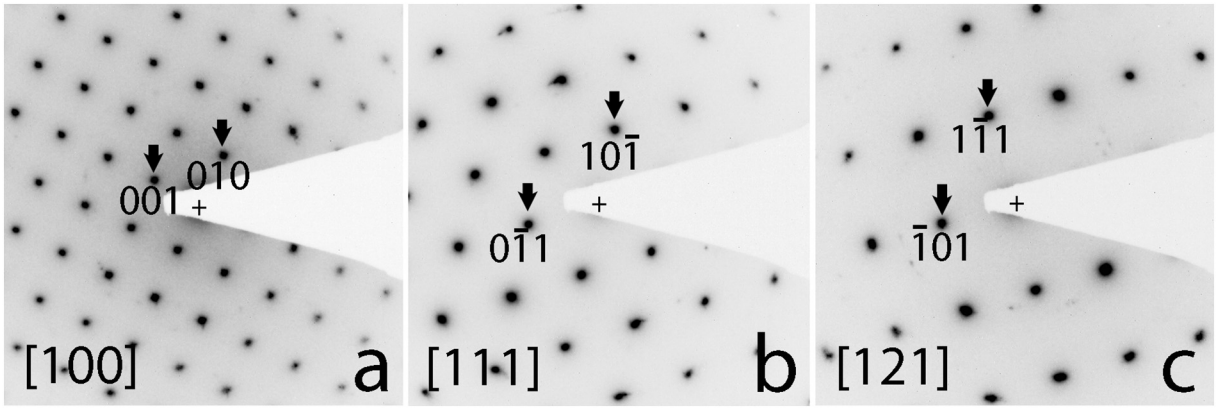

Fig. 7. SAED patterns of the Cr-rich phase in the 500 °C-annealed CoGeCrGe ribbons.

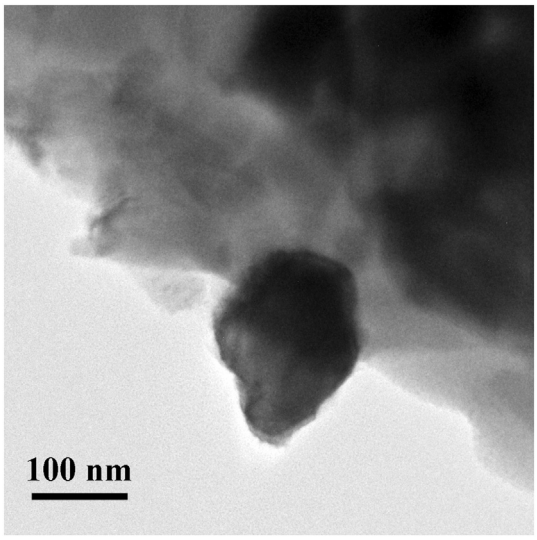

Fig. 8. TEM image of the new tetragonal phase in the 500 °C-annealed CoGeCrGe ribbons.

rich crystalline phases in Co-Cr, Fe-Cr, Fe-Ge alloy systems were explored. From the known crystalline phases in Table 1, a reasonable conjecture is that Cr and Ge are exchangeable in the crystalline structures, as well as Fe and Co. In this way, the composition of the new tetragonal phase may regroup as (Co, Fe) and (Cr, Ge).

4.2. Comparison of the Magnetic Hysteresis Loops of the 300 °C and 500 °C-Annealed Samples

The investigation on magnetic properties of 300 °C- and 500 °C-annealed samples was reported in the previous paper [7]. However, the details of magnetic hysteresis loops were overlooked. The experimental data are re-examined and interpreted with the help of the new tetragonal phase. Fig. 15 shows the magnetic hysteresis loops measured from (a) 300 °C- and (b) 500 °C-annealed samples. The hysteresis loop from 300 °C-annealed sample is a smooth curve of single-phase compound with its coercivity H_c = 65 Oe and saturation magnetization M_s = 525 emu/cm^3. This is in agreement with the $L2_1$ phase with partial chemical disorder. The hysteresis loop from the 500 °C-annealed sample has a kink curve of the two-phase composite with a coercivity H_c = 130 Oe and saturation magnetization M_s = 690 emu/cm^3, which cannot be attributed to the secondary Cr-rich cubic phase which consists of a total content of 10% of Fe and Co. The kink is due to the exchange coupling between the hard magnetic phase (the new tetragonal phase) and soft magnetic phase (the $L2_1$ phase with partial disorder or the B2 phase). This type of exchange coupling is also reported in the previous studies [19,20]. It is believed that the new tetragonal phase with a total content of 84% of Fe and Co is a hard magnetic phase, so that the hysteresis loop can be interpreted as the combined $L2_1$ phase with partial chemical disorder (or B2 phase) and the new tetragonal phase.

4.3. Synthesis of the New Tetragonal Phase

Although the ideal Heusler compound has a stoichiometric formal of X_2YZ, the $L2_1$ phase with partial chemical disorder in the quaternary Co-Fe-Cr-Ge system may exist in a range of compositions. Assuming that the composition of the samples is not completely homogenous, the $L2_1$ phase with partial chemical disorder can be formed in the as-spun and 300 °C-annealed samples. After annealing above 402 °C, the composition near equiatomic CoFeCrGe will keep the $L2_1$ phase with partial chemical disorder, and the composition away from CoFeCrGe forms two new phases, Cr_3Ge type and (CoFe)-rich tetragonal type.

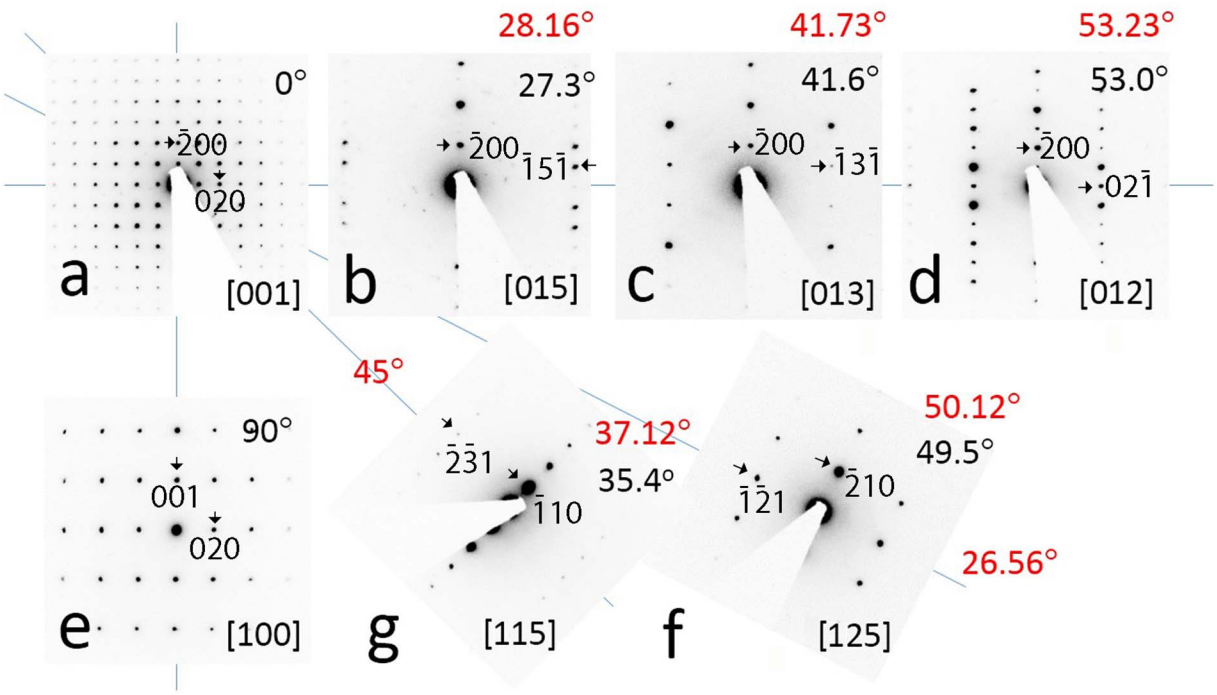

Fig. 9. SAED patterns of the new tetragonal phase in the 500 °C-annealed CoGeCrGe ribbons.

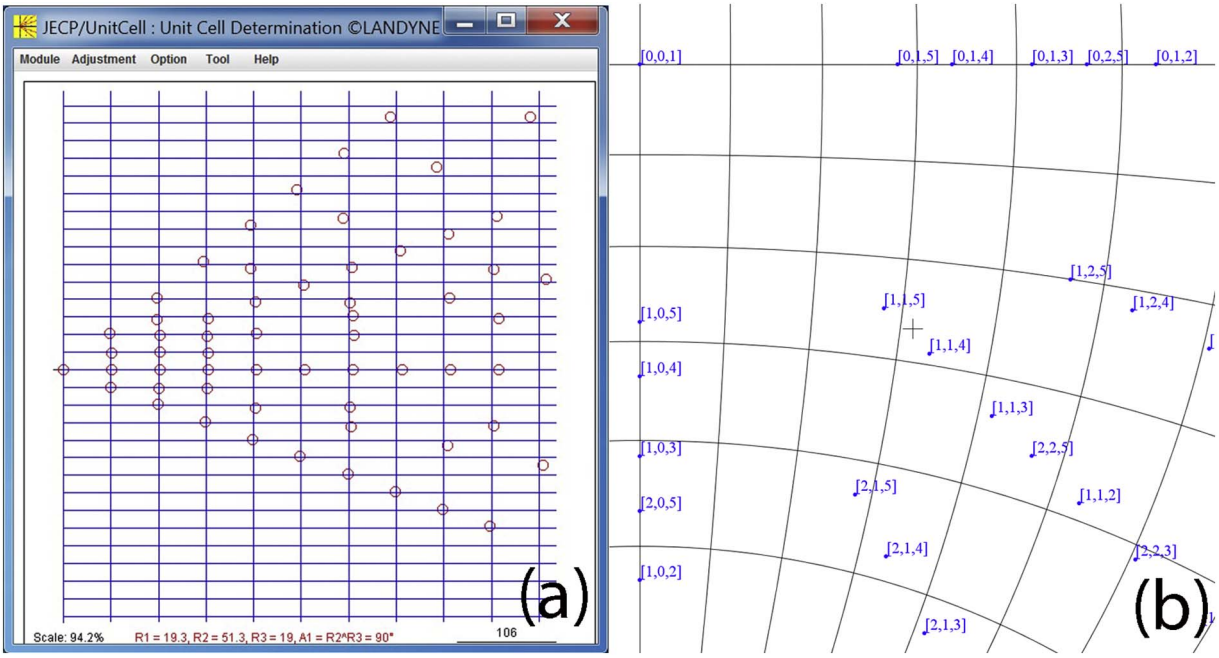

Fig. 10. (a) Lattice reconstruction and (b) stereogram of the new tetragonal phase in the 500 °C-annealed CoGeCrGe ribbons.

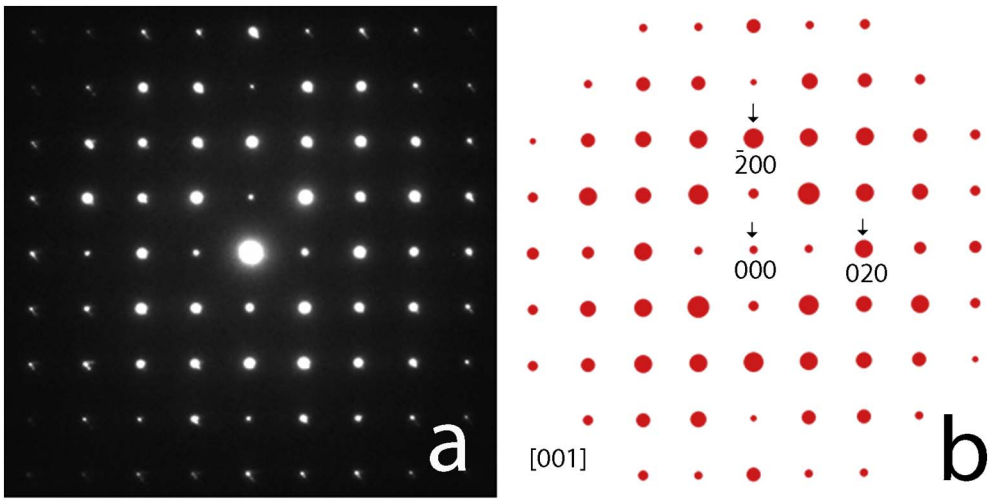

Fig. 11. (a) SAED pattern of the new tetragonal phase along [001] zone axis and (b) the processed intensities with averaged intensities of (hkl) and (-h -k -l).

Experiments regarding the synthesis of the single phase compound of the new tetragonal phase with a composition of $Co_{53.4}Fe_{30.4}Cr_{8.6}Ge_{7.6}$ and a slight variation have been carried out, but the structural analysis did not show a single phase. A possible reason is that the new tetragonal phase is not a crystalline phase in the equilibrium phase diagram and it can only exist as a metastable compound which is embedded in the $(Cr, Fe, Co)_3Ge$ matrix. In the further work, one of the possible compositions of the new tetragonal phase is suggested near the composition of $Co_{20.4}Fe_{14.4}Cr_{48.5}Ge_{16.7}$, which is obtained by combining 36% $Co_{3.8}Fe_{6.4}Cr_{68.5}Ge_{21.3}$ and 18% $Co_{53.4}Fe_{30.4}Cr_{8.6}Ge_{7.6}$. Elemental doping may also be a direction to develop the single tetragonal $Co_{53.4}Fe_{30.4}Cr_{8.6}Ge_{7.6}$ phase or to increase the amount of this phase.

5. Concluding Remarks

In this work, a structural study of the CoFeCrGe system has been systematically carried out for as-spun and annealed samples. The B2 structure was found in the as-spun samples and the main compound

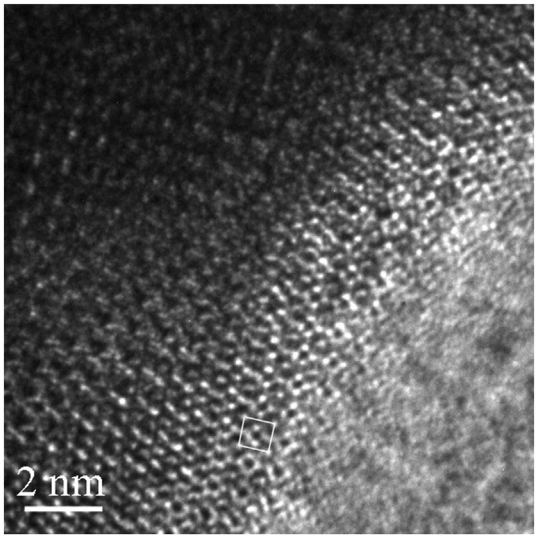

Fig. 12. HREM image of the new tetragonal phase along the [001] zone axis.

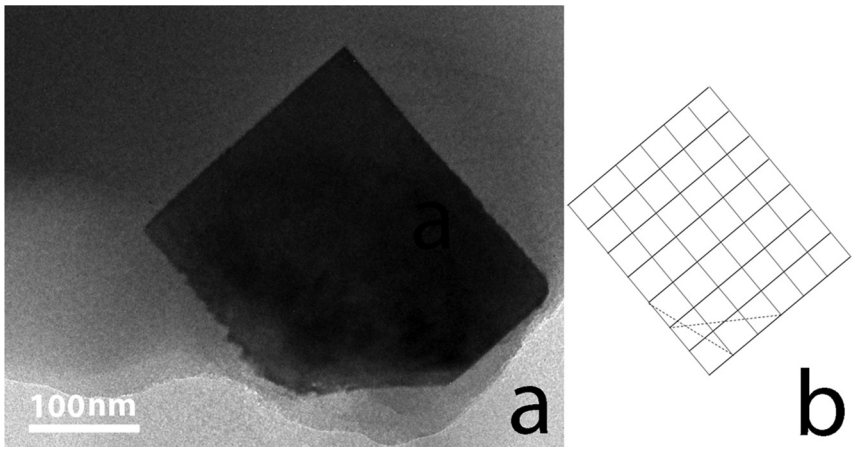

Fig. 13. (a) TEM image of the new tetragonal phase and (b) a schematic drawing for the interpretation of the facets of the grain.

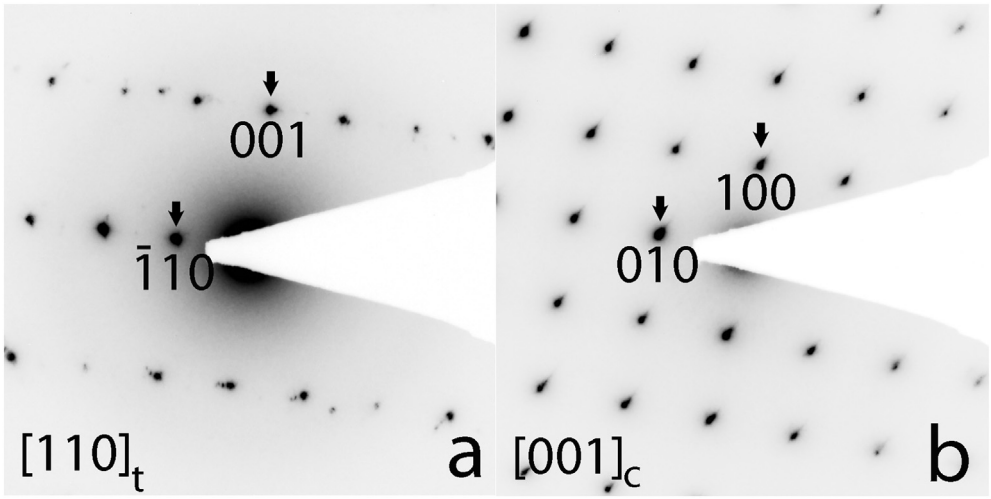

Fig. 14. SAED patterns of (a) the new tetragonal phase along the [110] zone axis and (b) the Cr-rich cubic phase along the [100] zone axis. In the experiment, a tilt angle of about 6.7° was found between (b) and (a).

Table 1
Selected crystalline phases in Co-rich and Fe-rich binary and (Co,Fe)-rich ternary systems.

Crystalline phase	Prototype	Space group	Lattice parameters (nm)	Reference
Co_3Cr	Ni_3Sn	$P6_3/mmc$ (194)	a = 0.5028; c = 0.4034	[14,15]
Fe_3Ge	Ni_3Sn	$P6_3/mmc$ (194)	a = 0.5169; c = 0.4222	[14,16]
Fe_3Cr	$MnAlCu_2$	Fm-3 m (225)	a = 0.5669	[17]
Co_2FeGe	$MnAlCu_2$	Fm-3 m (225)	a = 0.571	[18]
$(Co,Fe)_{83.8}(Cr,Ge)_{16.2}$		$P42_12$ (90)	a = 0.76; c = 0.284	This work

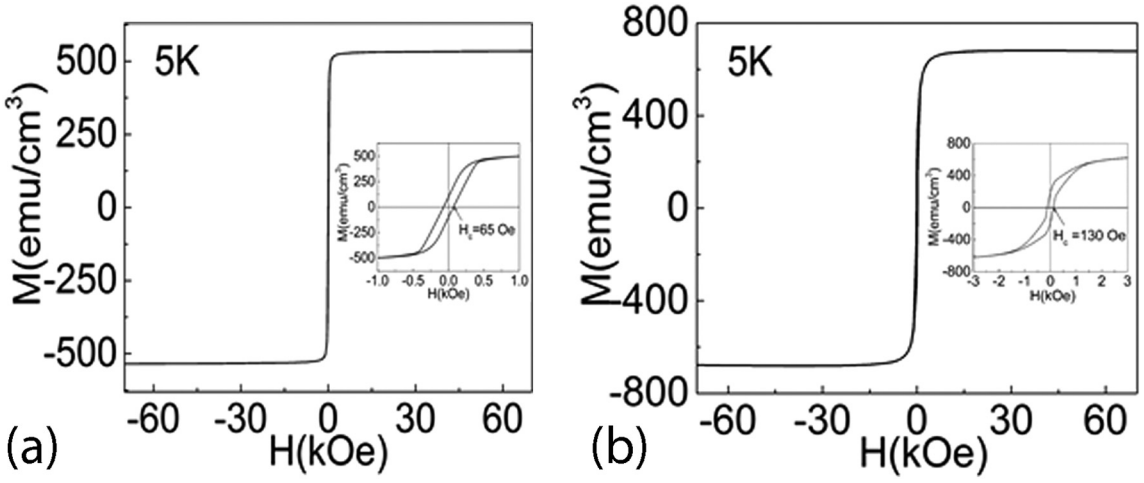

Fig. 15. Magnetic hysteresis loops measured from (a) the 300 °C– and (b) the 500 °C-annealed samples.

was found to be the $L2_1$ phase with partial chemical disorder and B2 structure in further disorder case in the annealed samples. In the 500 °C-annealed sample, two other compounds appear, which were identified as a Cr_3Ge-type phase and the new tetragonal phases. The lattice type and parameters of the new tetragonal phase have been determined in the experiment with a tilt series of SAED patterns. A comparison of magnetic hysteresis loops at the 300 °C-annealed and 500 °C-annealed sample is presented with the emphasis on the contribution from the new tetragonal phase. The possible reason for the formation of the new tetragonal phase was also discussed.

Acknowledgment

We would like to express our thanks to Prof. Wang and Dr. Nguyen at the Ames Laboratory for a discussion of the new tetragonal phase. This research was supported by NSF, DMR under Award DMREF: SusChEM 1436385. The research was performed in part in the Nebraska Nanoscale Facility: National Nanotechnology Coordinated Infrastructure and the Nebraska Center for Materials and Nanoscience, which are supported by the National Science Foundation under Award ECCS: 1542182, and the Nebraska Research Initiative.

References

[1] R.A. de Groot, F.M. Mueller, P.G.v. Engen, K.H.J. Buschow, Phys. Rev. Lett. 50 (1983) 2024.
[2] C. Felser, B. Hillebrands, J. Phys. D. Appl. Phys. 40 (2007) 3.
[3] X. Wang, G. Peleckis, C. Zhang, H. Kimura, S. Dou, Adv. Mater. 21 (2009) 2196.
[4] M.I. Katsnelson, V.Y. Irkhin, L. Chioncel, A.I. Lichtenstein, R.A. de Groot, Rev. Mod. Phys. 80 (2008) 315.
[5] H. Lin, L.A. Wray, Y. Xia, S. Xu, S. Jia, R.J. Cava, A. Bansil, M.Z. Hasan, Nat. Mater. 9 (2010) 546.
[6] D.P. Rai, A. Shankar, Sandeep, M.P. Ghimire, R.K. Thapa, J. Theor, Appl. Phys. 7 (2013) 3.
[7] Y. Jin, P. Kharel, P. Lukashev, S. Valloppilly, B. Staten, J. Herran, I. Tutic, M. Mitrakumar, B. Bhusal, A. O'Connell, K. Yang, Y. Huh, R. Skomski, D.J. Sellmyer, J. Appl. Phys. 120 (2016) 053903.
[8] H. Kurt, K. Rode, M. Venkatesan, P. Stamenov, J.M.D. Coey, Phys. Rev. B 83 (2011) 020405.
[9] J. Winterlik, S. Chadov, A. Gupta, V. Alijani, T. Gasi, K. Filsinger, B. Balke, G.H. Fecher, C.A. Jenkins, F. Casper, J. Kübler, G.-D. Liu, L. Gao, S.S.P. Parkin, C. Felser, Adv. Mater. 24 (2012) 6283.
[10] K. Özdoğan, E. Şaşıoğlu, I. Galanakis, J. Appl. Phys. 113 (2013) 193903.
[11] X.Z. Li, Microsc. Microanal. 22 (S3) (2016) 564.
[12] http://www.unl.edu/ncmn-cfem/xzli/computer-programs.
[13] X.Z. Li, J. Appl. Crystallogr. 49 (1818) (2016).
[14] P. Villars (Ed.), Pearson's handbook: Crystallographic Data for Intermetallic Phases, Desk edition, ASM international, 1998.
[15] A.K. Sinha, Trans. Metall. Soc. AIME 245 (1969) 237.
[16] J.-P. Turbil, Y. Billiet, A. Michel, Comptes Rendus Nebdomadaires des Seances del'Academie des Sciences, Serie C: Chimiques 269C (1969) 309.
[17] D. Connetable, M. Mathon, J. Lacaze, CALPHAD: Comput. Coupling of Phase Diag. Thermochem. 35 (588) (2011) (ICDD 01-082-8278).
[18] K.K. Ramesh, V.B. Babu, P.D. Kumar, N. Harish, AIP Conf. Proc. 1447 (1213) (2012) (ICDD 01-082-8750).
[19] Y. Liu, T.A. George, R. Skomski, D.J. Sellmyer, Appl. Phys. Lett. 99 (2011) 172504.
[20] Y. Jin, W.Y. Zhang, R. Skomski, S. Valloppilly, J.E. Shield, D.J. Sellmyer, J. Appl. Phys. 115 (17A739) (2014).